



Study of the influence of particle breakage on compression properties for carbonate sand

XinYue Zhu¹ · Sa Li¹ · YanBin Li² · TingTing Li¹ · JiangSong Yin¹

Received: 27 May 2021 / Accepted: 18 January 2022 / Published online: 9 February 2022
© Springer-Verlag GmbH Germany, part of Springer Nature 2022

Abstract

A series of one-dimensional compression tests up to 60 MPa were conducted to study the compression behavior and particle breakage for carbonate sand and quartz sand in different locations. The results show that at high stress, particle breakage is the main factor of compression, and the carbonate sand from South China Sea is the most compressible and easily crushed for its angular particle shape, smaller single particle strength, and higher calcium carbonate content. A relationship between applied stress and plastic work considering particle breakage was established by taking Hardin's relative breakage index B_r as an intermediate variable, and a compression model is developed which could describe the compression deformation caused by crushing. At the same time, the proposed model is also applicable to the whole compression process, and it could well describe the results of test in this paper and in previous studies.

Keywords Carbonate sand · One-dimensional compression · Particle breakage · Plastic work · Compression model

Introduction

Carbonate sand is a sediment composed of calcium carbonate or other insoluble substances. It is primarily distributed in tropical continental shelves and coastlines or sub-tropical regions (Holmes 1978). In recent years, the carbonate sand is widely used as foundation of buildings and roads or construction materials. Due to carbonate sand presents characteristics of high void ratio, irregular particle shape and high crushability (Semple 1988; Brandes 2011; Zhou et al. 2019), particle breakage significantly affects the deformation characteristics of carbonate sand which gives rise to a series of problems to foundation stability and engineering safety. Therefore, the compression caused by crushability of carbonate sand has been under active investigations by many researchers and engineers (McDowell 2002; Kikumoto et al. 2010; Al Hattamleh et al. 2013; Xiao et al. 2017; Lin et al. 2020).

In one dimensional compression, particle breakage is the main internal factor contributing to the reduction of volume. In order to investigate the influence of particle breakage on one dimensional compression, De Souza and Roberts (1958) first defined a yield point and stated that beyond which the particle breakage becomes significant through loading a high stress of 138 MPa. Later studies confirmed that the compression mechanism before and after the yield point could be considered as particle rearrangement and particle crushing, respectively (Roberts 1965; Hardin 1985; Coop 1990; Hagerty et al. 1993; McDowell and Bolton 1998; Chuhan et al. 2003; Wils et al. 2015). Moreover, Nakata et al. (2001) related the statistics of individual particle crushing with the compression line curvature, providing a more convincing understanding about the nature of compression for crushable soils. Xiao et al. (2017) established the empirical correlations between the Hardin's relative breakage index B_r with the changes in stress, strain, and input energy based on one-dimensional compression tests.

For crushable sand, such as carbonate sand, it is fundamental to have an understanding of the impact of particle breakage on soil compression behavior, which is expected to evaluate the foundation settlement accurately, especially when the soils are subjected to high stresses. Some of the existing compression models could be used to simulate the compressibility at high stress levels.

✉ Sa Li
lisa@tju.edu.cn

¹ School of Civil Engineering, Tianjin University, Tianjin, China

² China Energy Construction Group, Shanxi Electric Power Survey and Design Institute Co. Ltd, Taiyuan, China

Hardin (1987) defined a model of $\frac{1}{e} = \frac{1}{e_0} + \frac{1}{S_{1D}} \left(\frac{\sigma'_v}{p_a} \right)^P$, inspired by the linear relationship between $\frac{1}{e}$ and $\left(\frac{\sigma'_v}{p_a} \right)^P$ before yielding and S_{1D} is a constant at this stage; after yielding, S_{1D} varies with stress and should be determined by extra six parameters pertaining to soil crushability.

Pestana and Whittle (1995) developed an elaborated elasto-plastic model with four parameters through assuming that the tangent bulk modulus as the function of current void ratio (e) and effective stress (σ'_v), which successfully predicted the loading and unloading compression behavior.

Meidani et al. (2017) made an assumption of active and inactive void ratios whose decrease are induced by particle rearrangement and crushing respectively, and proposed a two-parameter model based on the linear relation between “ $de/d\sigma'_v$ ” and “ e ,” the model performs well when $\sigma'_v < 8$ MPa for calcareous sands. Nevertheless, it is still a problem worth studying to consider the impact of particle crushing on soil compression, especially under high pressure.

In this paper, based on one-dimensional compression tests under 60 MPa for the carbonate sand and quartz sand, the yield stress “ σ_b ” at yield point (De Souza and Roberts 1958) of different sand is determined. For the post-yield loading stage, i.e., $\sigma'_v > \sigma_b$, taking B_r as the intermediate variable, a compression model considering particle breakage is established. Experimental results show that the model is also applicable to the case where $\sigma'_v < \sigma_b$.

Materials and test procedure

Sample preparation

The carbonate sands tested in this paper are from South China Sea (SC) and Arabian Gulf (AG). In addition, a type of quartz sand (QZ) obtained from Tianjin, China is prepared for contrast. Figure 1 shows the scanning electron micrograph (SEM) of these sands. It can be seen that the sand particles of SC are most angular and contain a large amount of intraparticle voids. By contrast, the particles of AG are sub-angular with smooth surfaces, and the shape of the particles of QZ are similar to that of SC.

The chemical components of the sands are studied by energy-dispersive X-ray spectrometry (EDS), as shown in Table 1, the calcium carbonate content (CaCO_3) for sample SC, AG, QZ are 91.85%, 80.93%, and 4.73%, respectively. The predominant chemical compositions in the quartz sand are silica (SiO_2), with the value of 86.6%.

Five kinds of oven-dried specimens were prepared and tested, and the particle size distributions (PSD) are shown in Fig. 2. According to ASTM (2017), the tested specimens are

all poorly graded. SC1 and SC2 were carbonate sands from South China Sea with different medium grain sizes of 0.4, 0.15 mm; AG4 represented the carbonate sand from Arabian Gulf; SC3, which was graded identically with AG4, was made of the carbonate sand from South China Sea; QZ5, the quartz sand with the same PSD as that of SC1, was prepared for contrast with SC1.

The physical and single particle mechanical properties indexes of the tested materials are reported in Table 2 (ASTM 2014; ASTM 2016a; ASTM 2016b; ASTM C136 2019). Single particle crushing tests were carried out for 1–2-mm diameter selected from three kinds of sand. For each kind of sand, 30 particles are investigated, with reference to Nakata et al. (1999), McDowell and Amon (2000) and Xiao et al. (2020). The single particle strength σ is obtained according to the method proposed by Jaeger (1967),

$$\sigma = \frac{F}{d^2} \quad (1)$$

where F is the value of the maximum peak loading measured in the single particle crushing test. d is the distance between the platens at the start of the single particle crushing test. Taking the average value of 30 particles as the single particle strength σ .

As seen in Table 2, the largest single particle strength is quartz sand, followed by Arabian Gulf sand, and South China Sea carbonate sand. In addition, the values of Mohs hardness are cited from Mohs (1825).

Since this test mainly studies the impact of particle crushing on compression, the tested sands in this study were air dried sands. The tested specimens were 61.8 mm in diameter and 20 mm in height. Each specimen was designed to compress at $D_r = 45\%$, 60%, and 75% prepared by the tapping method of Ladd (1978). Air dried sand was divided into two layers, the solid mass for each layer m_L at a given relative density D_r is calculated as:

$$D_r = \frac{(\rho_d - \rho_{dmin})\rho_{dmax}}{(\rho_{dmax} - \rho_{dmin})\rho_d} \quad (2)$$

$$m_L = \frac{\rho_d V}{2} \quad (3)$$

where ρ_d is the dry density of specimen at given relative density; ρ_{dmax} , ρ_{dmin} are the maximum and minimum dry density, respectively; V is the volume of specimen.

Then, each layer was placed into the mold lined with 0.3-mm-thick rubber membrane through a zero-drop-height funnel. To ensure the uniformity of specimen, the first layer is compacted to a lower density, of which the height is designed as 10~11.5 mm, then the second layer is placed

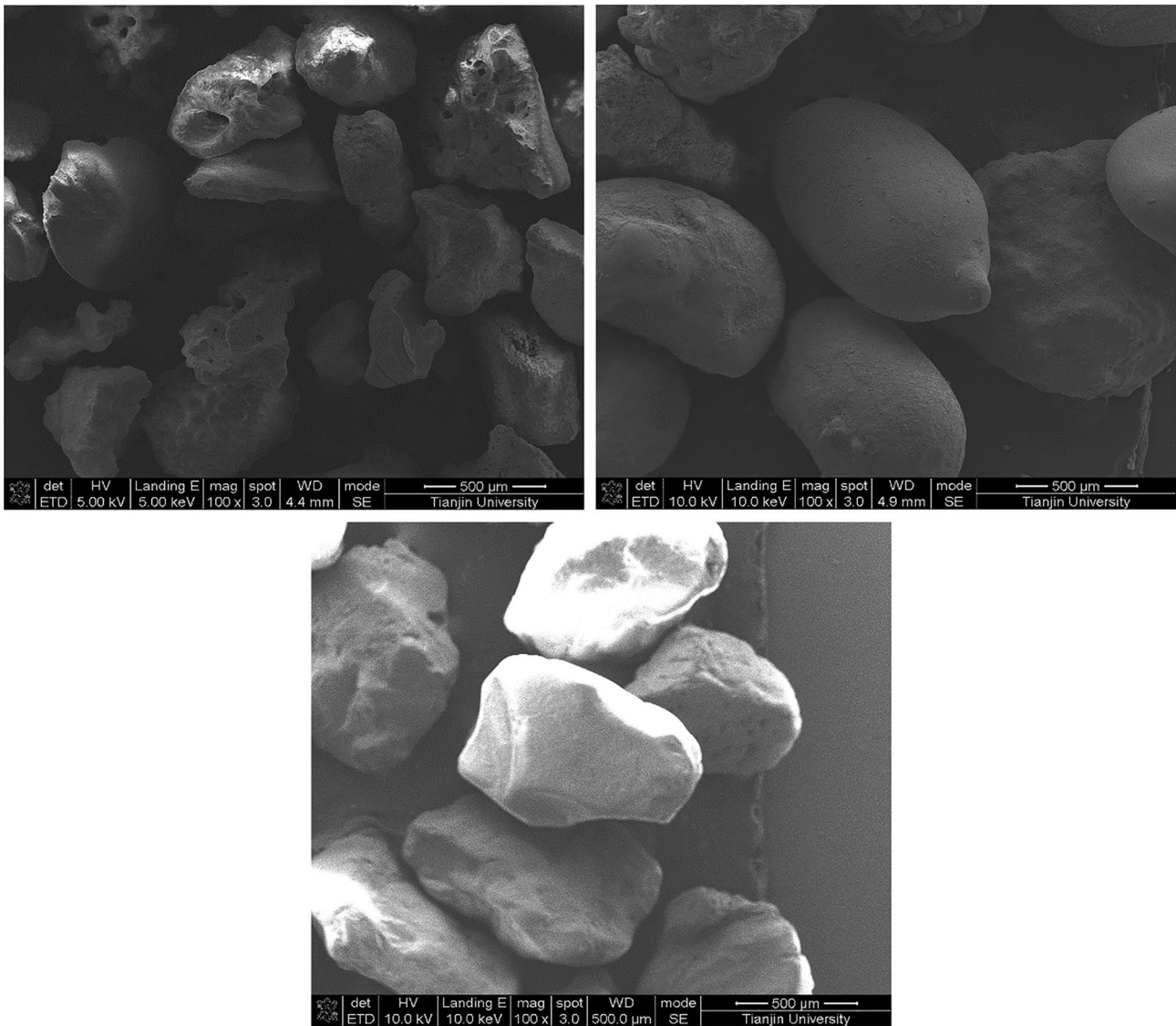


Fig. 1 Scanning electron microscopy (100×) of tested sands: **a**) carbonate sand of South China Sea, **b**) carbonate sand of Arabian Gulf, and **c**) quartz sand

and compacted to the height of 20 mm. The target height of each layer was achieved by tapping the mold with a rubber hammer. The actual relative densities used in tests and following analyses are illustrated in Table 3.

Table 1 Chemical components of test samples

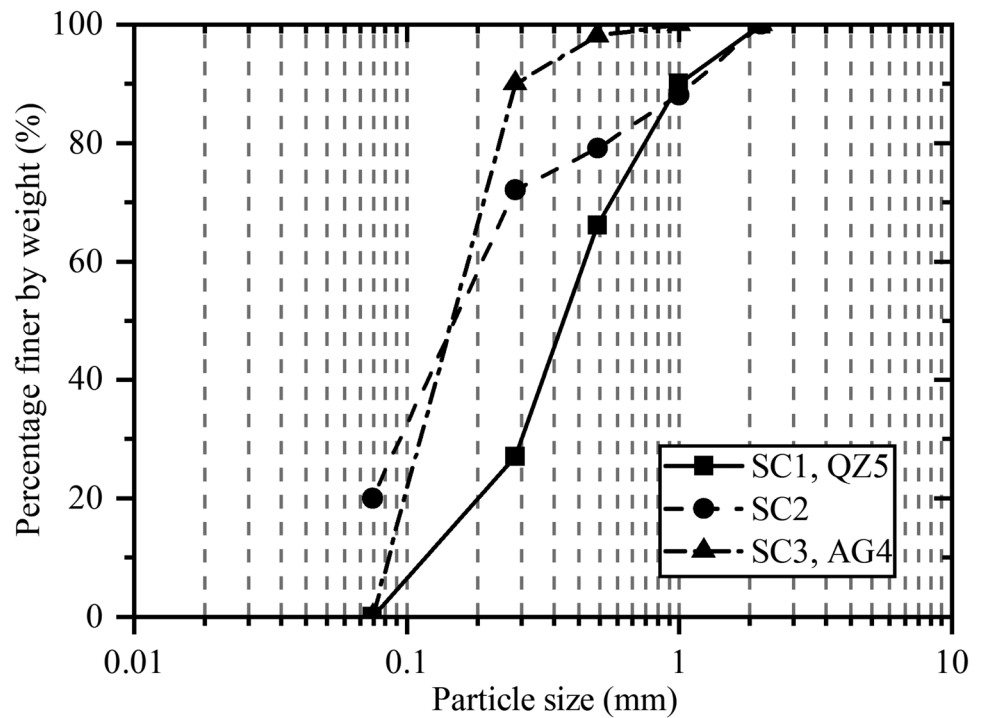
Specimen name	Mass percentage, %				
	CaCO ₃	Al ₂ O ₃	Fe ₂ O ₃	MnO	SiO ₂
SC1	91.85	0.9876	2.995	0.0286	4.13
SC2					
SC3					
AG4	80.93	2.54	2.844	0.0895	13.59
QZ5	4.73	6.108	2.564	-	86.6

Test procedure

A series of one-dimensional compression tests were carried out by the high pressure oedometer located in the Institute of Geotechnical Engineering, Tianjin University and performed according to ASTM (1996). The tests were conducted on the specimens of SC1, SC2, SC3, AG4, and QZ5 at three initial relative densities about 45%, 60%, and 75% to the target vertical effective stress of 60 MPa to get the compression properties of soils.

To investigate the particle crushing with increasing stress, additional tests were conducted on the specimens with the initial relative density of 60%. In these tests, six terminated stress levels of 2.0, 4.0, 6.0, 10, 20, and 40 MPa were applied, whose test series number are SC1-2, SC2-2,

Fig. 2 Original particle size distributions of tested specimens



SC3-2, AG4-2, and QZ5-2. After each test, specimens were poured out carefully and followed by particle sieving for the analysis of PSD. Table 3 presents a summary of all the tests conducted.

Results and discussion

One-dimensional compression behavior

The experimental $\sigma'_v - \epsilon_v$ curves for tested specimens with different relative densities, subjected to the elevated vertical effective stress of 60 MPa, are shown in Fig. 3a, c, and e. All the trend lines represent that volumetric strain increases with an increase of σ'_v , and at a given stress, the volumetric strain is less for each specimen with higher initial relative density. The corresponding $e - \log \sigma'_v$ curves are plotted in Fig. 3b,

d, and f. Notably, it could be found that the $e - \log \sigma'_v$ curves for each specimen with different initial relative densities converge into a unique line, which is called the limiting compression curve (LCC) by Pestana and Whittle (1995), indicating that the effect of initial relative density on compression is eliminated at relatively high stresses.

Different characteristics of sands from different locations

Figure 3a and b compare the compression behavior for specimens SC1 and SC2, of which the medium grain sizes are 0.4 mm and 0.15 mm, respectively. From $\sigma'_v - \epsilon_v$ curves, the produced volumetric strain of SC2 is less than that of SC1 at a given σ'_v , no matter what the initial relative density is. This phenomenon could be explained by more preexisting fissures and crystal imperfections in larger grain size

Table 2 Physical and mechanical properties of tested samples

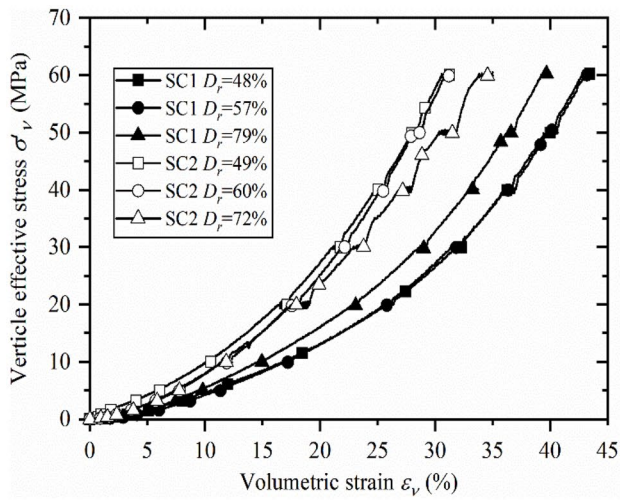
Specimen name	Specific gravity, G_s	Medium grain size, d_{50} (mm)	Uniformity coefficient, C_u	Curvature coefficient, C_c	ρ_{dmax} (kg/m ³)	ρ_{dmin} (kg/m ³)	Mohs hardness*	Single particle strength (1–2 mm) (MPa)
SC1	2.79	0.40	3.20	1.10	1.523	1.205	3	15.3
SC2	2.79	0.15	3.15	1.20	1.853	1.393		
SC3	2.79	0.13	3.35	1.08	1.569	1.234		
AG4	2.79	0.13	3.35	1.08	1.806	1.522		17.9
QZ5	2.65	0.40	3.20	1.10	1.863	1.541	7	22.5

*The values are referenced from Mohs (1825)

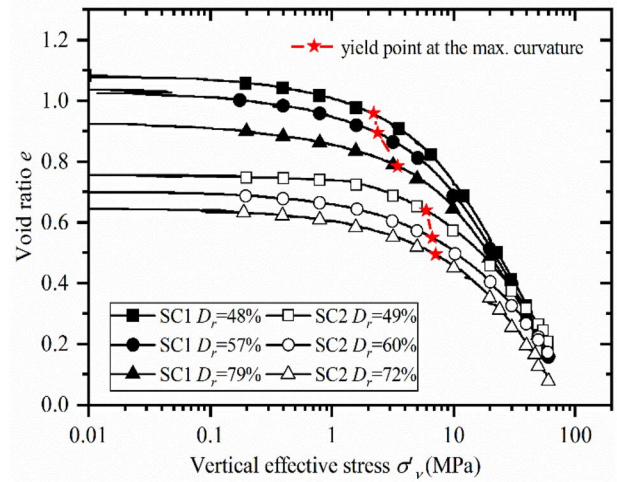
Table 3 Test settings and results

Specimen name	Test series	D_r (%)	Terminated stress σ'_v (MPa)	Relative breakage index, B_r (%)	Total input work, W_p (MPa)	Yield stress σ_b (MPa)	W_{p1} (MPa)
SC1	SC1-1-60	48	60	37.27	8.428	2.2	0.055
	SC1-2-60	57	60	36.93	8.539	2.4	0.060
	SC1-3-60	79	60	35.97	7.668	3.5	0.093
	SC1-2-2	57	2	2.81	0.043	-	-
	SC1-2-4	56	4	5.03	0.140	-	-
	SC1-2-6	57	6	6.34	0.269	-	-
	SC1-2-10	57	10	9.37	0.680	-	-
	SC1-2-20	56	20	18.10	1.962	-	-
	SC1-2-40	58	40	29.48	5.234	-	-
SC2	SC2-1-60	49	60	19.57	6.912	6.0	0.221
	SC2-2-60	60	60	19.89	6.240	6.7	0.249
	SC2-3-60	72	60	22.00	7.642	7.1	0.261
	SC2-2-2	60	2	1.91	0.024	-	-
	SC2-2-4	61	4	3.68	0.107	-	-
	SC2-2-6	60	6	4.23	0.205	-	-
	SC2-2-10	60	10	5.80	0.533	-	-
	SC2-2-20	59	20	8.99	1.462	-	-
	SC2-2-40	60	40	15.60	3.651	-	-
SC3	SC3-1-60	38	60	24.94	8.619	3.5	0.086
	SC3-2-60	53	60	21.47	7.712	3.8	0.096
	SC3-3-60	79	60	21.37	8.582	6.0	0.068
	SC3-2-2	54	2	1.19	0.040	-	-
	SC3-2-4	54	4	3.29	0.109	-	-
	SC3-2-6	55	6	4.81	0.214	-	-
	SC3-2-10	53	10	6.19	0.523	-	-
	SC3-2-20	54	20	8.73	1.686	-	-
	SC3-2-40	53	40	15.77	4.818	-	-
AG4	AG4-1-60	46	60	16.95	6.620	13.0	0.411
	AG4-2-60	60	60	16.80	6.358	14.1	0.488
	AG4-3-60	71	60	16.57	6.427	14.6	0.438
	AG4-2-2	60	2	1.07	0.008	-	-
	AG4-2-4	61	4	1.54	0.069	-	-
	AG4-2-6	60	6	2.01	0.137	-	-
	AG4-2-10	61	10	3.06	0.317	-	-
	AG4-2-20	60	20	7.03	0.976	-	-
	AG4-2-40	61	40	14.35	3.278	-	-
QZ5	QZ5-1-60	33	60	14.60	6.549	12.8	0.477
	QZ5-2-60	60	60	14.17	6.309	17.7	0.664
	QZ5-3-60	71	60	13.75	5.213	18.4	0.758
	QZ5-2-2	60	2	0.85	0.016	-	-
	QZ5-2-4	59	4	1.11	0.039	-	-
	QZ5-2-6	60	6	1.62	0.074	-	-
	QZ5-2-10	61	10	4.14	0.215	-	-
	QZ5-2-20	60	20	6.09	0.889	-	-
	QZ5-2-40	60	40	11.28	3.310	-	-

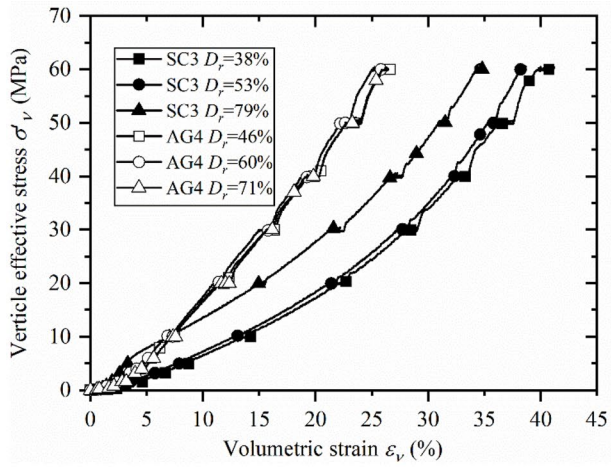
The tests are numbered according to the initial relative density and target vertical effective stress. For example, test SC1-2-60 indicates the specimen SC1 with the second kind of initial medium; relative density was subjected to the terminal vertical effective stress of 60 MPa



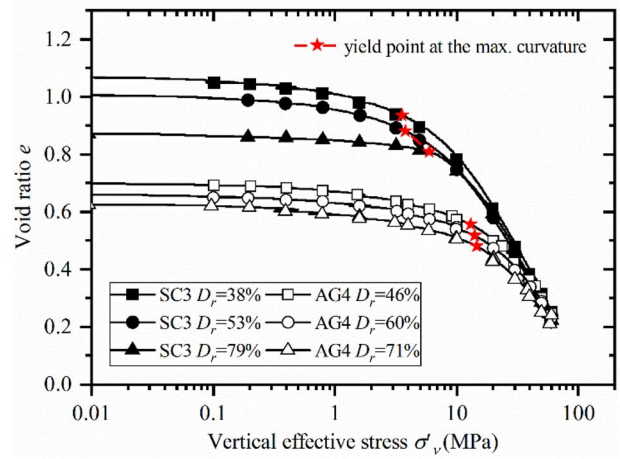
(a)



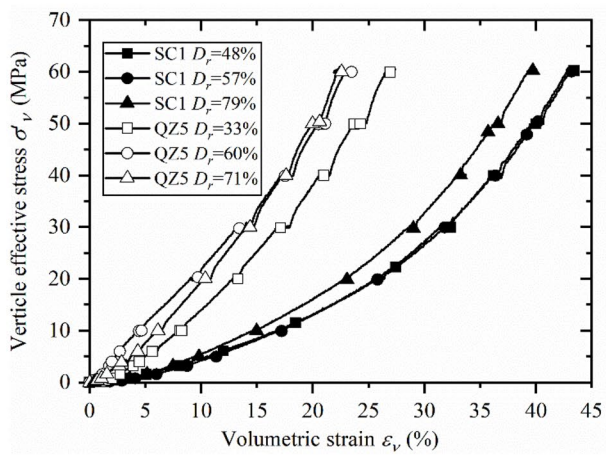
(b)



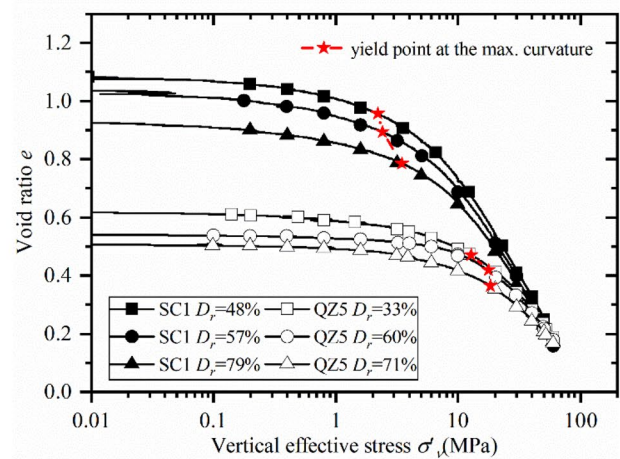
(c)



(d)



(e)



(f)

Fig. 3 One-dimensional compression behavior for five specimens: (a), (c), (e) volumetric strain versus vertical effective stress curves; (b), (d), (f) void ratio versus vertical effective stress curves

particles, so it could be easily crushed (Zhang et al. 1990; Chuhan et al. 2003).

Comparisons are made between specimens SC3 and AG4 with the same grading curve (Fig. 3c, d), which are both the carbonate sand based on the classification system in Clark and Walker (1977), but located in different marine areas of South China Sea and Arabian Gulf, respectively. It was obvious that during the whole loading process, the volumetric strain of SC3 is larger than that of AG4 no matter what the initial relative density is. When the stress increases to 60 MPa, the highest total volumetric strain of SC3 compressed at three initial relative densities up to 40%, and that of AG4 is 27%, indicating that the carbonate sand of South China Sea would experience more deformation and be easily compressed than the carbonate sand of Arabian Gulf. The differences may come from different calcium carbonate content, different particle angularity, and single particle strength.

In addition, comparisons between SC1 and QZ5 are showed in Fig. 3e and f. It could be found that the increasing of ϵ_v with σ'_v is obviously faster in carbonate sand than in quartz sand, and the maximum final volumetric strain of QZ5 is 27%, which is much smaller than that of SC1 up to 44%. Moreover, from the $e - \log \sigma'_v$ curves, the void ratio of QZ5 decreases much slowly before 10 MPa than that of SC1, which further validates that carbonate sand has higher compressibility than that of quartz sand due to the large amount of particle breakage, which is validated later in this paper.

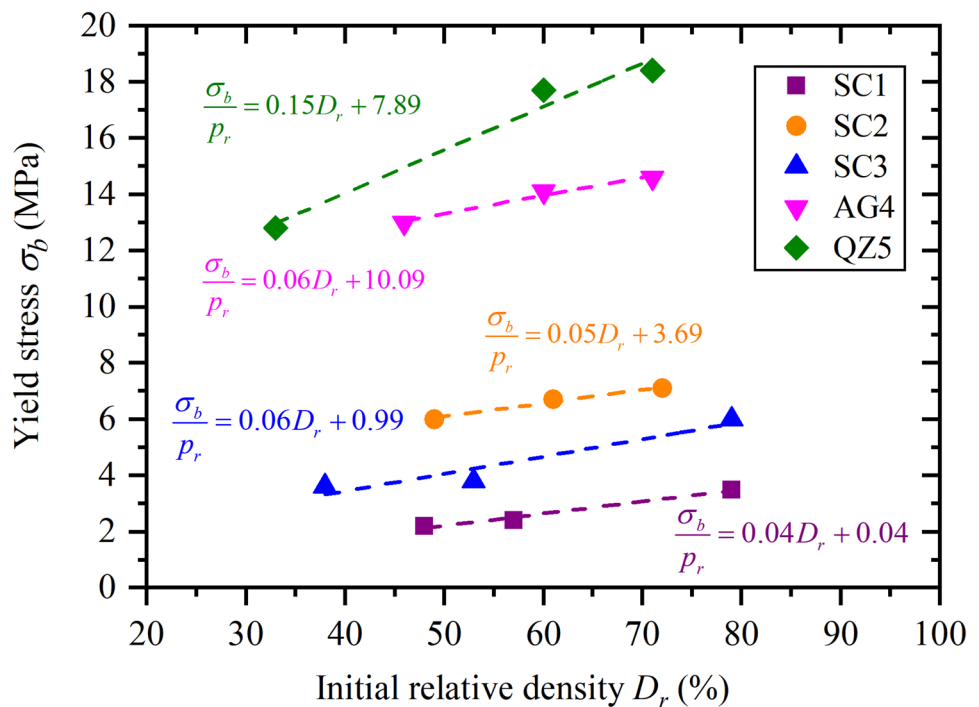
Yield stress determined from the $e - \log \sigma'_v$ plot

The “yield point” defined by De Souza and Roberts (1958) was determined as the point of maximum curvature in the $e - \log \sigma'_v$ curves. The yield points in tests are shown in Fig. 3 (marked as red star symbols), and the corresponding yield stresses σ_b are listed in Table 3.

Figure 4 shows the relationship between the yield stress σ_b with respect to the initial relative density for each sand specimen. Apparently, a strong positive linear relation could be observed between the two variables, that is, the particle crushing initiates at a much lower stress in loose sand than in dense sand. This can be explained by the fact that the coordination number increases with increasing relative densities. Particles are imposed on smaller average contact stress for the large amount of particle contacts in a denser configuration, which results in the ability of resisting particle crushing intensifies (Hendron Jr 1963; Coop and Lee 1992; Mesri and Vardhanabhuti 2009).

Moreover, the figure shows that the carbonate sands from South China Sea have the lower yield stresses, and the yield stresses of QZ5 and AG4 are obviously higher than those of carbonate sand specimens SC1 and SC3, though they have the same PSDs. Combining the analysis of compression behavior in Fig. 3, it could be found that a low yield stress is significative of high compressibility.

Fig. 4 Linear correlation between the yield stress and initial relative density for five specimens. (p_r is the reference pressure with the value of 1 MPa)



Particle size distributions and particle crushing

After tests, the PSD curves are plotted in Fig. 5 to determine the particle breakage. In this study, the relative breakage index B_r , proposed by Hardin (1985) was used to assess particle breakage. B_r is defined as,

$$B_r = \frac{B_t}{B_p} \quad (4)$$

where B_p is the breakage potential, which is determined by the area between the initial gradation curve, and the vertical line representing the lower limit of particle size $d=0.074$ mm; B_t is the total breakage, equal to the area between the initial and final gradation curves (Fig. 6).

The relative breakage index B_r , determined from the grading curves in Fig. 5 is listed in Table 3. Figure 5a (1–5) shows the PSD before and after 60 MPa applied under different initial relative density. It could be found that the initial relative density has almost no effect on the amount of broken particles at the end of the test, which is different with that at low stress levels proposed by Xiao et al. (2017). This fact demonstrates that the effect of initial relative density on compression will be reduced and eventually eliminated when subjected to high stresses. In addition, at 60 MPa, the relative breakage index B_r of SC1 is the largest, reaching 36%, significantly higher than that of SC2 ($B_r = 18\%$) and SC3 ($B_r = 21\%$), which are both carbonate sand from South China sea but with smaller medium grain size; the relative breakage index B_r of AG4 is 16.5%, smaller than that of same graded specimen SC3 ($B_r = 21\%$). For the relative breakage index B_r of QZ5, it is much smaller ($B_r = 14\%$) than that of the same graded specimen SC1 ($B_r = 36\%$). It is because that carbonate sand has more angular particle shape, smaller single particle strength, and higher calcium carbonate content, which are recognized as the internal factors that lead to the high crushability of carbonate sand (Nakata et al. 2001; Wang et al. 2021).

The evolutions of PSD for test series of SC1-2, SC2-2, SC3-2, AG4-2, and QZ5-2 with the relative density about 60% are shown in Fig. 5b (1–5). For each given specimen, the PSD curves appear a gradual change deviating from the initial grading curve, indicating that particle breakage extent intensifies as the stress increases.

The relationship between B_r and vertical effective stress σ'_v is shown in Fig. 7. It could be found that the curve of specimen SC1 lies high alone departing from other curves since its B_r is much larger than that of other specimens at each given stress, implying the great particle crushability of SC1. From the enlarged graph, it can be seen that at low stress levels, the trend lines of SC1, SC2, and SC3 are convex upward which are different from that of AG4 and QZ5, this might be due to that the carbonate sand from South

China Sea would experience significant particle crushing even at the low stress compared to the Arabian Gulf's sand and quartz sand.

Many people have studied the evolution of B_r with the changes in applied stress subjected to one-dimensional compression or isotropic compression, the fitting form including power-law, inverse-exponential law, and hyperbolic function (Yan and Shi 2014; Mun and McCartney 2017; Xiao et al. 2017). The inverse-exponential form is used in this paper:

$$B_r = \alpha [1 - \exp(-\beta \sigma'_v)] \quad (5)$$

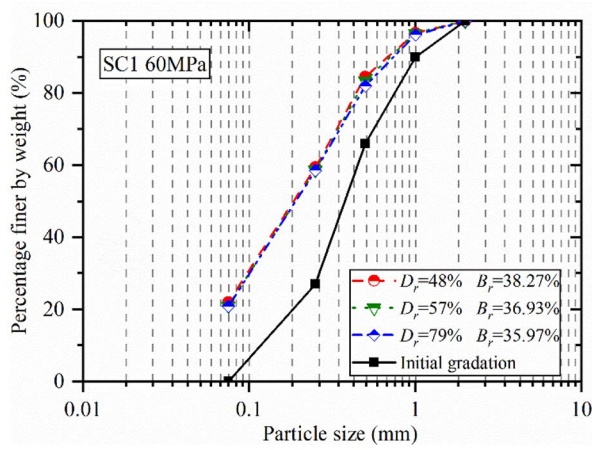
where α and β are material coefficients. As $\sigma'_v \rightarrow \infty$, then $B_r \rightarrow \alpha$. It means that a limit state of particle breakage exists, which is consistent with the discussion of breakage mechanics in Einav (2007). For the parameter β , when $\beta \rightarrow 0$, then $B_r \rightarrow 0$. It means that when particles do not break, the B_r of soil tends to 0. The fitting curves (dashed lines) for each specimen are plotted in Fig. 7, and the values of α and β are listed in Table 4 with good R^2 value varying from 0.9759 to 0.9987.

From Figs. 3 and 7, it could be found that the more particle breakage is subjected, the greater the compressibility of soil, which can be explained by the fact that the initially compression in sand is limited due to grain-scale frictional slip, rotation, and sliding. But if the effective stress is high enough, crushing of the particles becomes prominent, which could generate large relative motions between sand particles, consequently result in large deformation (e.g., De Souza and Roberts 1958; Hagerty et al. 1993; Chuhan et al. 2003; Al Hattamleh et al. 2010).

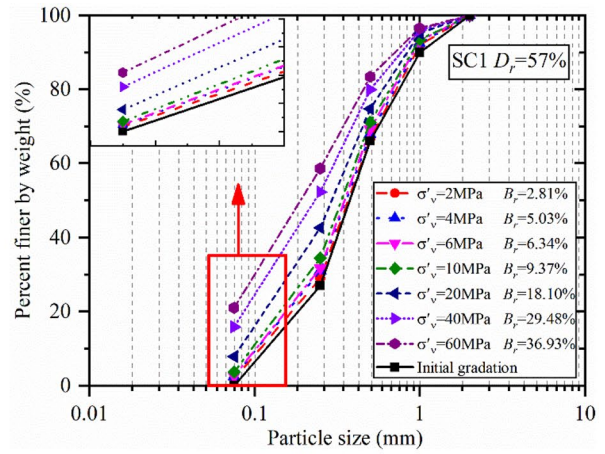
A compression model for crushable sand

Derivation of the compression model for post-yield stage

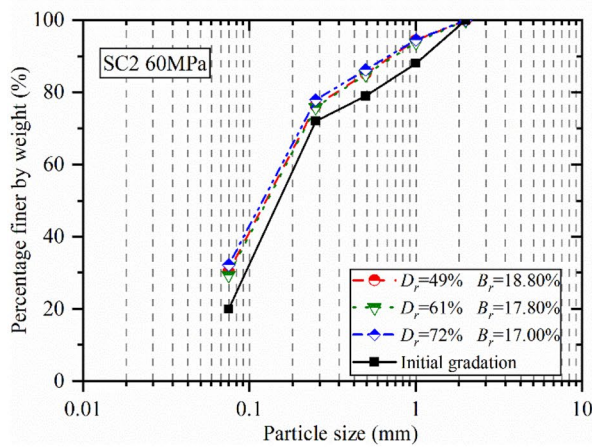
The plastic work is considered as a comprehensive index that incorporates the material characteristics including grain size distribution, grain strength, and particle shape, as well as the stress level (Yu 2017). The relationship between the plastic work and particle breakage is concerned by many people. Miura and Sukeo (1979) proposed an S-type model to describe the increasing trend of surface area with the plastic work per unit volume for triaxial test; Lade et al. (1996) derived a new crushing parameter B_{10} and correlated it with the total input energy per unit volume in a hyperbolic model; Wu et al. (1997) discovered a unique correlation between the relative breakage index B_r and the plastic work based on the triaxial tests for artificial calcareous sands, regardless of the test conditions and stress paths; moreover, Xiao and Liu



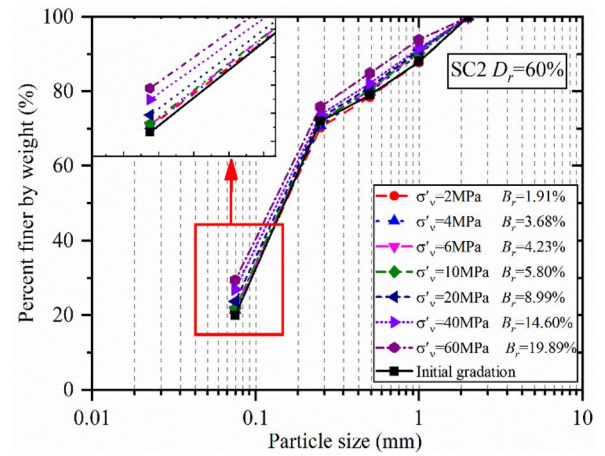
(a₁)



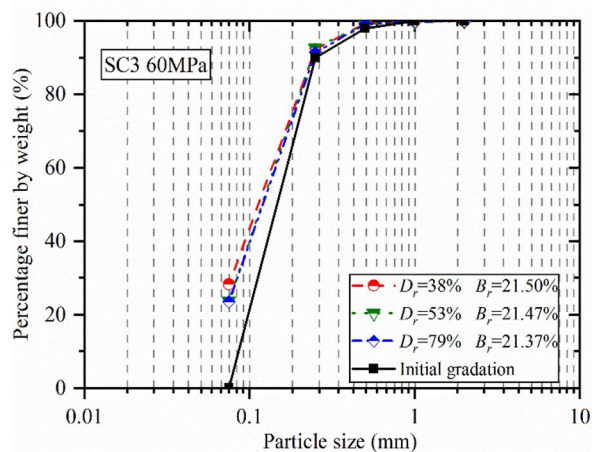
(b₁)



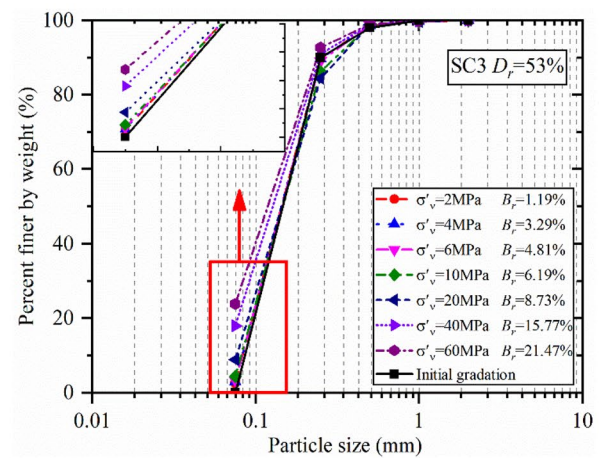
(a₂)



(b₂)

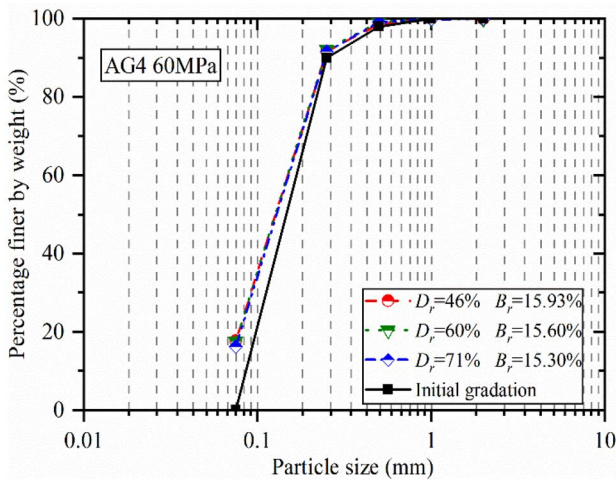


(a₃)

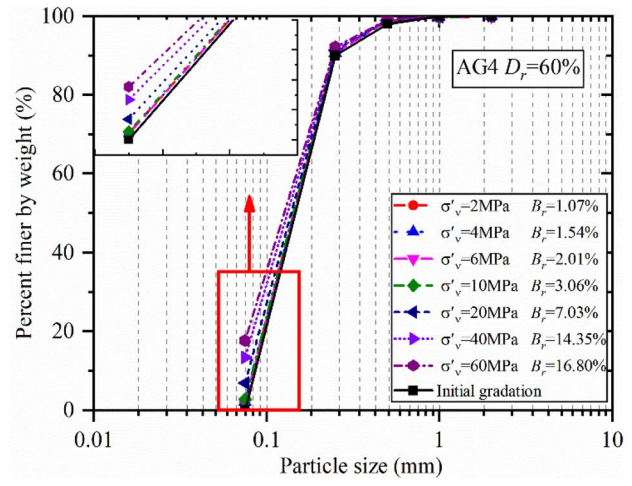


(b₃)

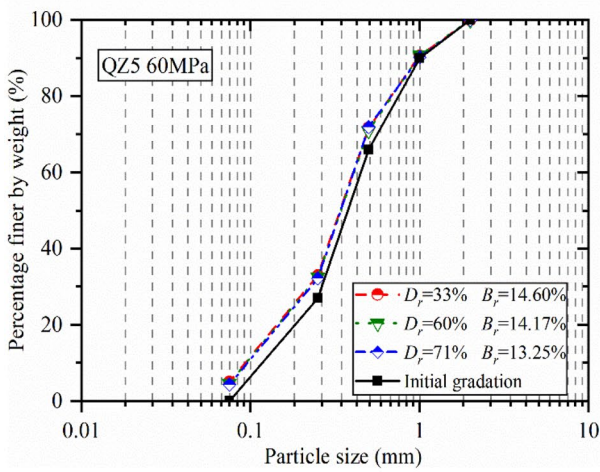
Fig. 5 Evolutions of particle size distribution (a): with different initial relative densities at the high stress up to 60 MPa; (b): with increasing stress at the medium relative density



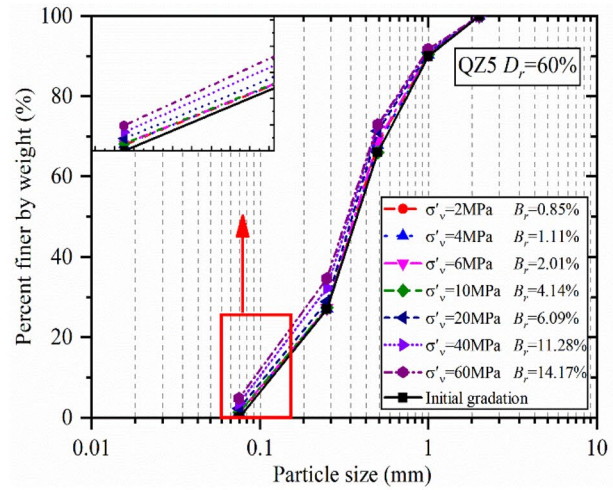
(a₄)



(b₄)



(a₅)



(b₅)

Fig. 5 (continued)

(2017) defined a breakage factor pertain to d_{50} for rockfill materials during triaxial loading and made a correlation with the plastic work in an exponential function.

During one dimensional compression, the incremental plastic work per unit volume is defined as:

$$dW_p = \sigma'_v d\varepsilon_v - \sigma'_{ve} d\varepsilon_{ve} \tag{6}$$

where ε_v and ε_{ve} are the total volumetric strain and elastic volumetric strain and σ'_v is the vertical effective stress. In general, the magnitude of elastic volumetric strain is so small compared to the total volumetric strain that can be neglected for dry granular soils, especially when subjected to significant particle crushing. Therefore, Eq. (6) can be simplified as:

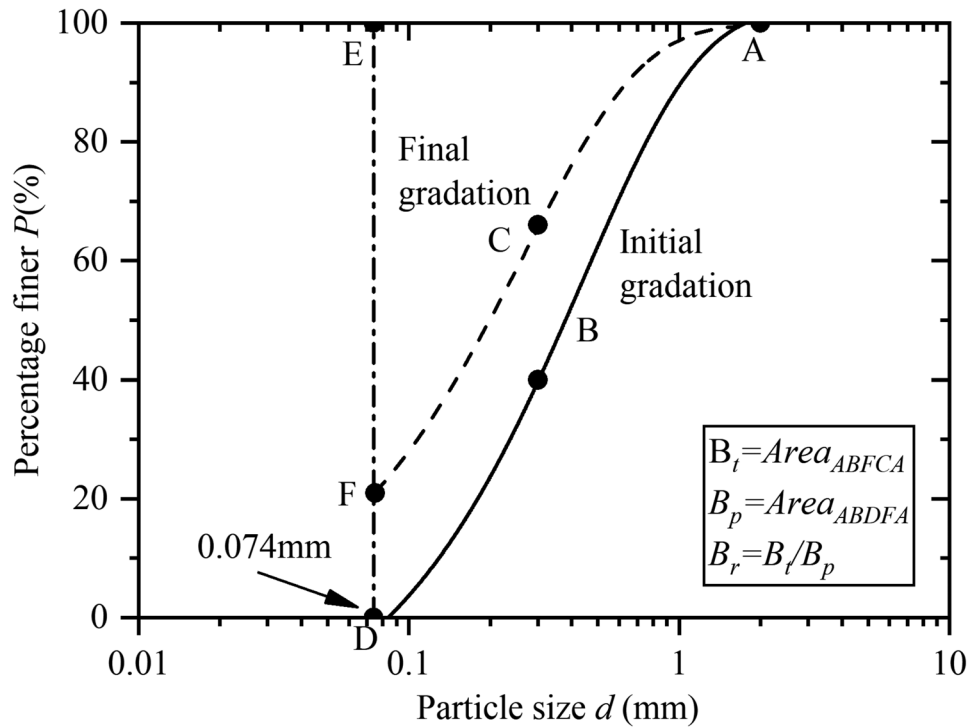
$$dW_p = \sigma'_v d\varepsilon_v \tag{7}$$

The total volumetric strain ε_v could be divided into two components, termed as ε_{v1} and ε_{v2} , which are produced before and after yielding mainly resulted from particle movements to adjust particles position and particle breakage, respectively. It means,

$$\varepsilon_v = \varepsilon_{v1} + \varepsilon_{v2}, \varepsilon_{v1} \in [0, \varepsilon_b), \varepsilon_{v2} \in [\varepsilon_b, \varepsilon_c) \tag{8}$$

Combining the terms ε_{v1} and ε_{v2} with Eq. (7), the corresponding plastic work W_{p1} and W_{p2} can be obtained, which represent the plastic works inputted before and after the yield stress, see Fig. 8. It could be expressed as,

Fig. 6 Definition of relative breakage index B_r (Hardin 1985)



$$W_p = W_{p1} + W_{p2}$$

$$(9) \quad W_{p2} = \int_{\epsilon_b}^{\epsilon_c} \sigma'_v d\epsilon_{v2} \quad (11)$$

$$W_{p1} = \int_0^{\epsilon_b} \sigma'_v d\epsilon_{v1}$$

(10) in which ϵ_b is the volumetric strain at the yield stress σ_b .
Because W_{p2} is the plastic work mainly for particle breakage, there could be a relationship between the particle

Fig. 7 Variations of the relative breakage index with increasing terminated stress for five specimens

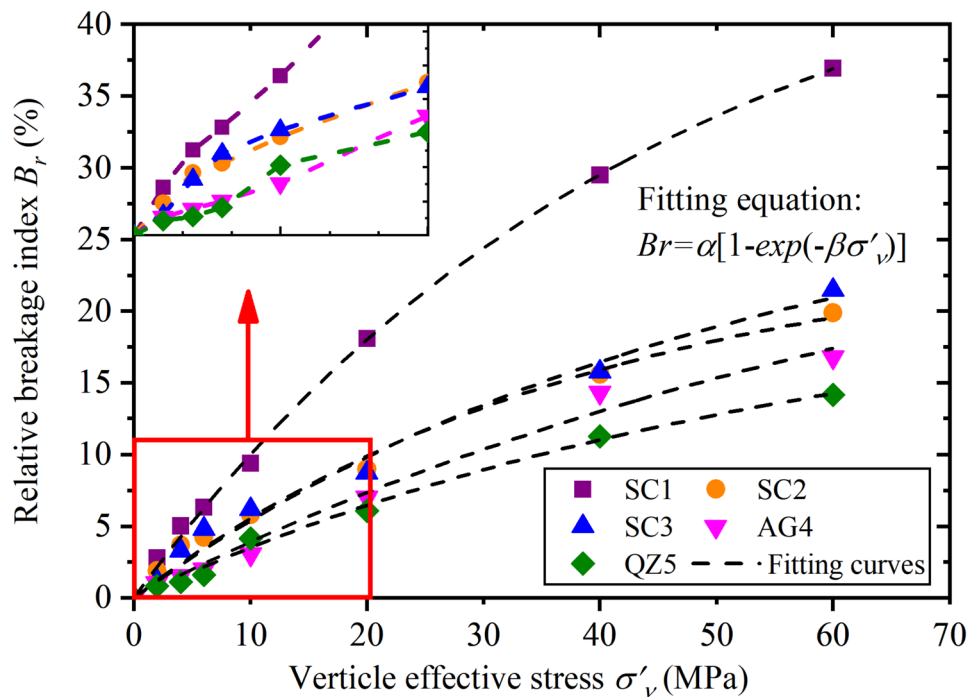


Table 4 Values of parameters

Function	Parameter	SC1	SC2	SC3	AG4	QZ5
$B_r = \alpha [1 - \exp(-\beta \sigma'_v)]$	α	49.92	26.90	30.33	30.76	20.89
	β	0.0224	0.0213	0.0196	0.0138	0.0190
	R^2	0.9987	0.9817	0.9775	0.9759	0.9911
$B_r = \kappa (W_{p2})^\lambda$	κ	13.20	8.96	8.55	9.48	8.88
	λ	0.483	0.443	0.416	0.339	0.264
	R^2	0.9970	0.9911	0.9591	0.9751	0.9979
$W_p = A [1 - \exp(-\beta \sigma'_v)]^\Gamma$	A	15.71	11.96	20.98	32.20	25.54
	B	0.0224	0.0213	0.0196	0.0138	0.019
	r	2.070	2.257	2.404	2.950	3.788

breakage B_r and W_{p2} . In this paper, the model proposed by Wu et al. (1997) is used,

$$B_r = \kappa (W_{p2})^\lambda \tag{12}$$

It could be written as

$$W_{p2} = F(B_r) = \left(\frac{B_r}{\kappa}\right)^{\frac{1}{\lambda}} \tag{13}$$

where κ, λ are parameters.

Figure 9 shows the relationship between the relative breakage index B_r and the corresponding plastic work W_{p2} for five specimens whose relative density is about 60%. From the figure it could be found that the proposed model can better express the relationship between them. The value of κ, λ are listed in Table 4. The coefficient λ reflects the rate of increase and therefore represents the crushability of tested

specimens, that is, the more crushable the specimen is, the larger value of λ would be obtained.

Substitute Eq. (5) into Eq. (13), the relationship between W_{p2} and σ'_v can be induced through making the relative breakage index B_r as the transitional variable.

$$\begin{aligned} W_{p2} &= \left(\frac{\alpha}{\kappa}\right)^{\frac{1}{\lambda}} [1 - \exp(-\beta \sigma'_v)]^{\frac{\Gamma}{\lambda}} \\ &= A [1 - \exp(-\beta \sigma'_v)]^\Gamma, \sigma'_v \geq \sigma_b \end{aligned} \tag{14}$$

where $A = \left(\frac{\alpha}{\kappa}\right)^{\frac{1}{\lambda}}, B = \beta, \Gamma = \frac{\Gamma}{\lambda}$, the values of A, B, Γ are listed in Table 4. Although B_r does not show up, this equation reflects the energy used for particle breakage at a given vertical effective stress.

Figure 10 shows the evolution of the plastic work W_{p2} with the vertical effective stress σ'_v at three initial relative

Fig. 8 Schematic diagram of the calculation of the plastic work

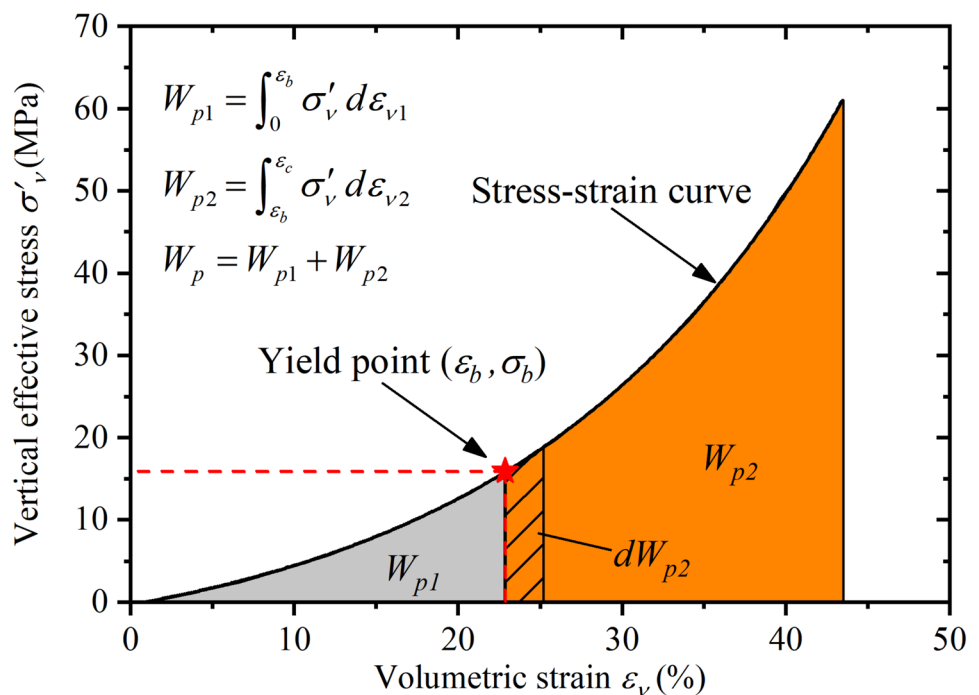
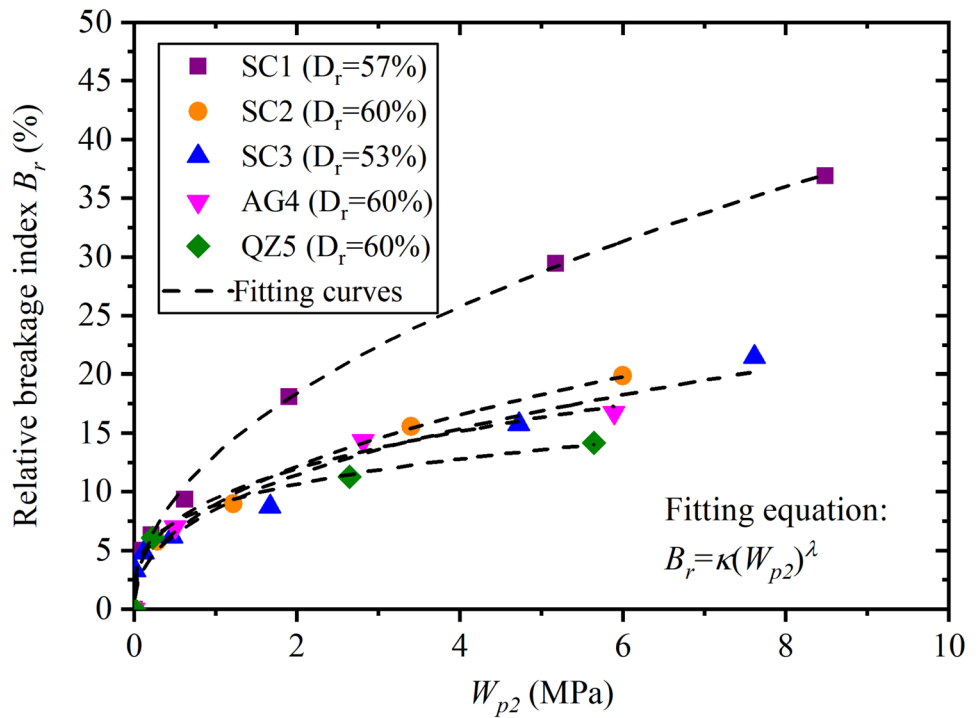


Fig. 9 Relationship between the relative breakage index and the plastic work W_{p2} for five specimens



densities for five specimens. All the regression parameters R^2 exceed 0.99, illustrating that Eq. (14) gives an excellent fitting to the experimental results.

Meanwhile, for one dimensional compression, the incremental volumetric strain $d\varepsilon$ is expressed by the incremental void space as

$$d\varepsilon = -\frac{de}{1 + e_0} \tag{15}$$

in which e_0 is the initial void ratio. At the same time, the void ratio e for loading can be written as a function of the vertical effective stress σ'_v

$$e = f(\sigma'_v) \tag{16}$$

then the incremental volumetric strain can be given by

$$d\varepsilon = -\frac{f'(\sigma'_v)}{1 + e_0} d\sigma'_v \tag{17}$$

Introducing Eqs. (14) and (17) into Eq. (11) yields

$$A[1 - \exp(-\beta\sigma'_v)]^\Gamma = W_{p2} = -\frac{1}{1 + e_0} \int_{\sigma_b}^{\sigma'_v} \sigma'_v f'(\sigma'_v) d\sigma'_v, \sigma'_v > \sigma_b \tag{18}$$

then taking the derivative of the vertical effective stress on both sizes of the equation, follows:

$$\frac{de}{d\sigma'_v} = f'(\sigma'_v) = -AB\Gamma \frac{1 + e_0}{\sigma'_v} \exp(-B\sigma'_v) [1 - \exp(-B\sigma'_v)]^{\Gamma-1}, \sigma'_v > \sigma_b \tag{19}$$

e_0 is the initial void ratio. A, B, Γ are model parameters. To this end, Eq. (19) can well describe the change of void ratio by particle breakage.

Taking SC2 ($D_r = 60\%$) as an example, Fig. 11 shows the relationship between the total plastic work W_p and σ'_v , the red star in this figure represents the yield point. The dashed line in the figure uses the model of Eq. (14) (the same as that in Fig. 10b). A, B, Γ are consistent with the values listed in Table 4. It can be seen that when $\sigma'_v > \sigma_b$, a good match can be obtained. But in the range of $\sigma'_v \leq \sigma_b$, the fitted value is significantly higher than the tested value, for the reason that the effect of crushing is taken into account in Eq. (14), which overestimates the plastic work without crushing.

The compression model for whole stage

It can be seen from the above analysis that the compression deformation caused by particle crushing can be better described by plastic work using B_r as an intermediate variable. Considering that the compression deformation caused by particle position adjustment can also be expressed by plastic work (W_{p1}), therefore the form of Eq. (14) is also used to describe the $W_p - \sigma'_v$ curve in the whole range of stress,

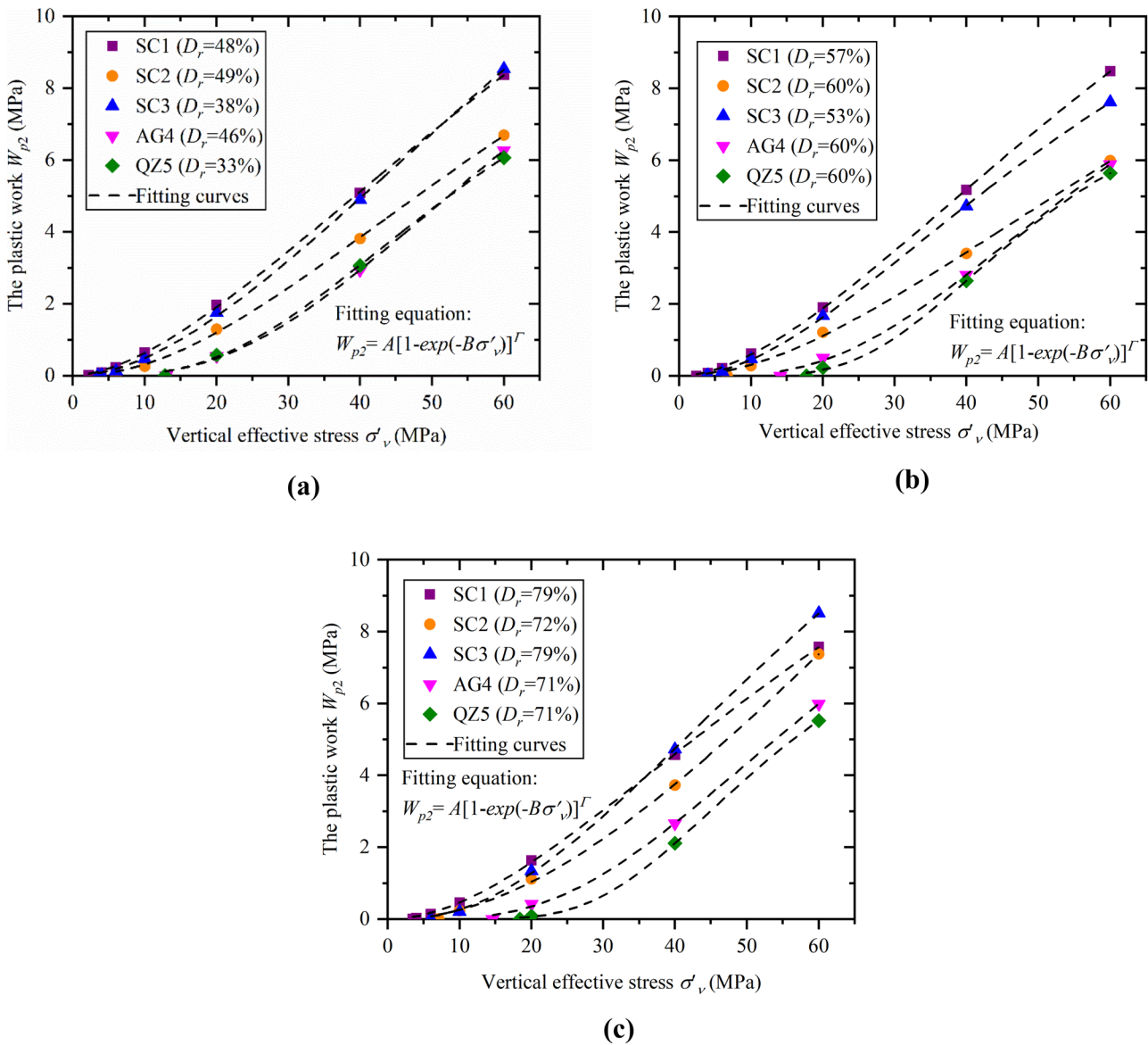


Fig. 10 Evolution of the W_{p2} with the vertical effective stress at three initial relative densities for five specimens

and the parameters are obtained by data fitting method. The fitting results are shown in Fig. 12. As can be seen from the figure, a good fitting can be obtained with all the coefficients R^2 exceed 0.999 (Table 5).

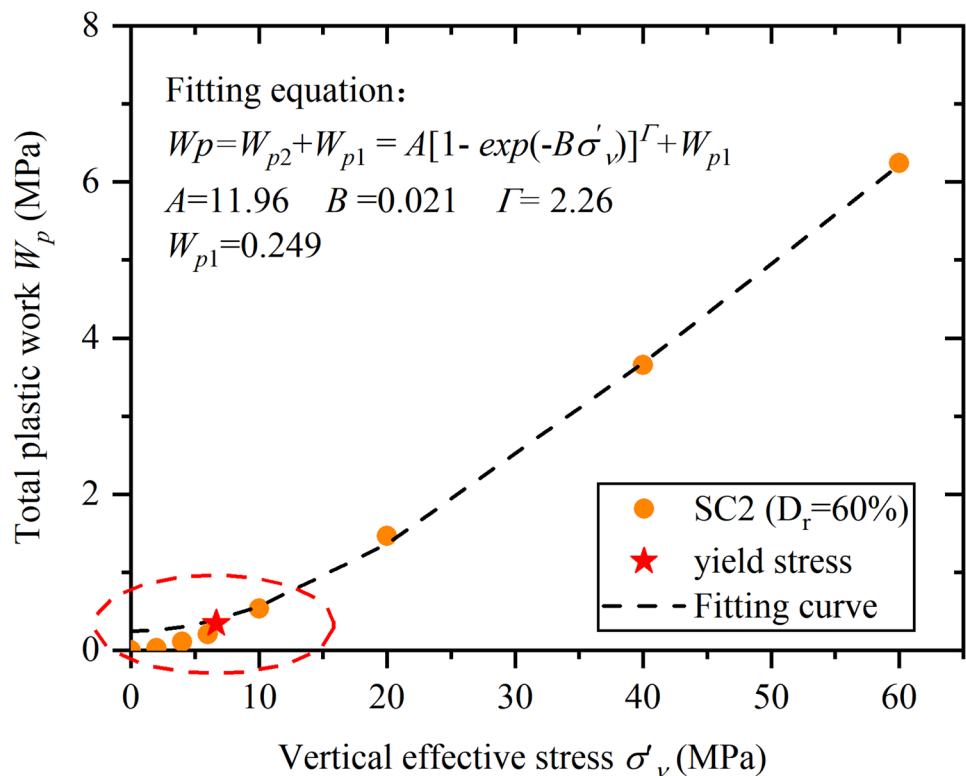
Herein, the three parameters are rewritten as A_r, B_r, Γ_r from data fitting for $W_p - \sigma'_v$ to distinguish from the corresponding parameters A, B, Γ from breakage evaluation for $W_{p2} - \sigma'_v$ curves. To this end, it could be convincible to give the compression model for the whole stress range of validity, as

$$\frac{de}{d\sigma'_v} = -A_r B_r \Gamma_r \frac{1 + e_0}{\sigma'_v} \exp(-B_r \sigma'_v) [1 - \exp(-B_r \sigma'_v)]^{\Gamma_r - 1}, \sigma'_v > 0 \tag{20}$$

From which, it has only three parameters pertaining to sand properties and can be numerically integrated from the initial loading condition ($\sigma'_v \rightarrow 0, e_0$), eluding the extra procedure to identify the yielding point on each compression curves. In addition, it could be observed that as $\sigma'_v \rightarrow \infty$, the extreme condition induce the same result of $\frac{de}{d\sigma'_v} \rightarrow 0$, implicitly reflecting the existence of asymptotic void ratios at extremely high stresses.

The one dimensional compression lines described by Eq. (20) with the three model parameters listed in Table 5 are compared to experimental results for the five tested specimens at three initial relative densities in semi-logarithmic

Fig. 11 Evolution of the total plastic work W_p with vertical effective stress (SC2-2)



space. As can be seen in Fig. 13, the model lines agree very well with the experimental data.

In addition, 8 groups of sands presented in previous literatures are used to verify the proposed model, see Fig. 14. It could be found that all the model curves have a good match with the data points, regardless of the mineral, grain size, gradation, initial density, single particle strength, showing a flexibility of the proposed model in capturing the compression behavior for a wide range of sands. The physical characteristics of sands used and model parameters are summarized in Table 6.

Discussion of the model parameters

In this paper, B_r is used as an intermediate variable to establish a compression model considering particle breakage, i.e., Eq. (19) for post-yield stage. In this equation, the three parameters A , B , Γ can be derived from the breakage behavior of soil directly, i.e., the parameters are from the relationship of $B_r - \sigma'_v$ and $B_r - W_{p2}$.

Figure 15 illustrates the rationality of this method by taking SC1-2 as an example. The blue line represents the

relationship between e and $\log \sigma'_v$ obtained by the proposed method with the data from $\sigma'_v < 20$ MPa. The red line shows the relationship between e and $\log \sigma'_v$ obtained by data fitting method with the data from $\sigma'_v < 20$ MPa. It can be seen that the compression behavior of $\sigma'_v < 20$ MPa can be well described by the proposed method and the data fitting method. But there is a big gap between the predicted results and the test results when $\sigma'_v > 20$ MPa for data fitting method when the test data were absent for fitting. However, the relationship between e and $\log \sigma'_v$ obtained from the evaluation of particle breakage behavior have a good performance to predict the compression behavior of soil when $\sigma'_v > 20$ MPa.

At the same time, the form of the compression model (Eq. 19) can also be extended to the whole loading range (0–60 MPa in this study) whose model parameters (A_r , B_r , Γ_r) need to be obtained by data fitting. To this end, the model proposed (Eq. 20) in this study can better describe the test results, but its accuracy in predicting the compressibility of soil beyond the test range needs to be further confirmed.

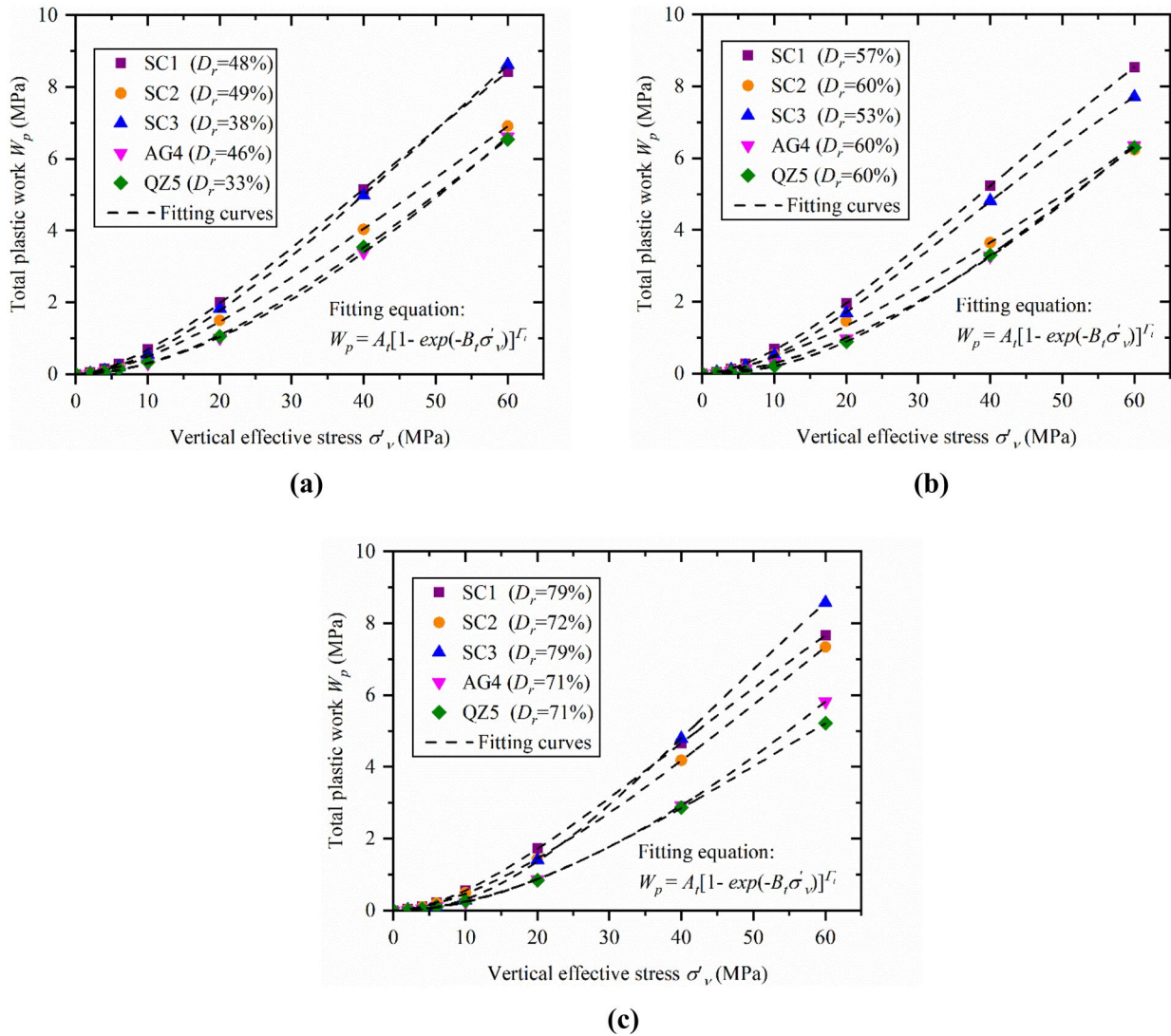
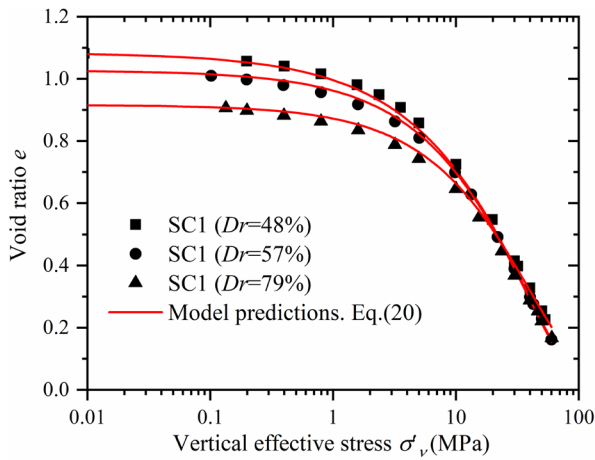


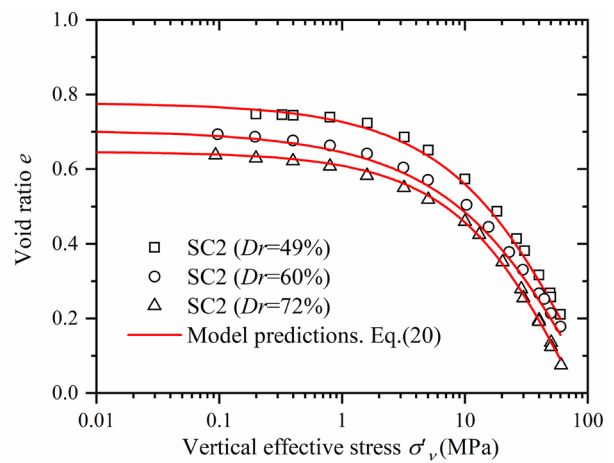
Fig. 12 Evolution of the total plastic work W_p with the vertical effective stress at three initial relative densities for five specimens

Table 5 Summary of input parameters for the tested specimens in this paper

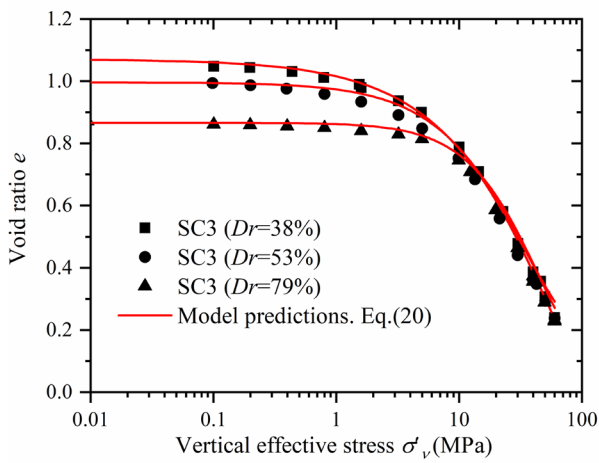
Sample name	Test series	D_r (%)	Initial void ratio e_0	Model parameters			R^2
				A_i	B_i	Γ_i	
SC1	SC1-1-60	48	1.0832	24.81	0.0123	1.6588	0.9999
	SC1-2-60	57	1.0411	22.74	0.0141	1.7405	0.9999
	SC1-3-60	79	0.9322	19.97	0.0147	1.7978	0.9999
SC2	SC2-1-60	49	0.7570	34.73	0.0076	1.6477	0.9999
	SC2-2-60	61	0.7037	43.35	0.0059	1.5842	0.9999
	SC2-3-60	72	0.6466	35.87	0.0085	1.7275	0.9999
SC3	SC3-1-60	38	1.0758	33.10	0.0103	1.7457	0.9999
	SC3-2-60	53	1.0065	15.38	0.0208	2.0330	0.9999
	SC3-3-60	79	0.8764	20.15	0.0205	2.4660	0.9999
AG4	AG4-160	46	0.6993	124.83	0.0037	1.8062	0.9999
	AG4-2-60	60	0.6600	119.41	0.0036	1.7980	0.9999
	AG4-3-60	71	0.6283	161.83	0.0029	1.8225	0.9999
QZ5	QZ5-1-60	33	0.6224	32.92	0.0096	1.9497	0.9999
	QZ5-2-60	60	0.5411	21.93	0.0148	2.3429	0.9999
	QZ5-3-60	71	0.5088	19.33	0.0125	2.0545	0.9999



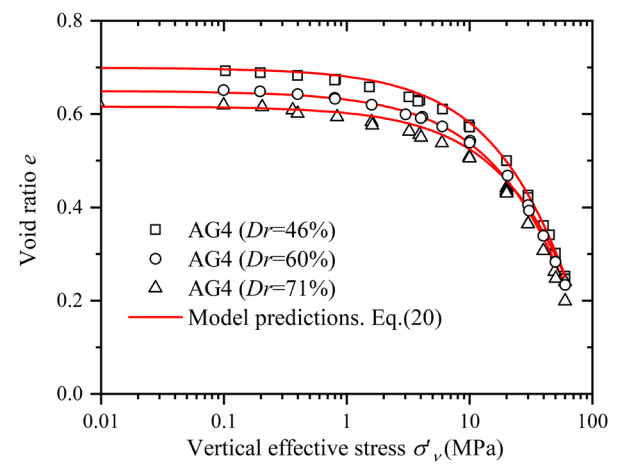
(a)



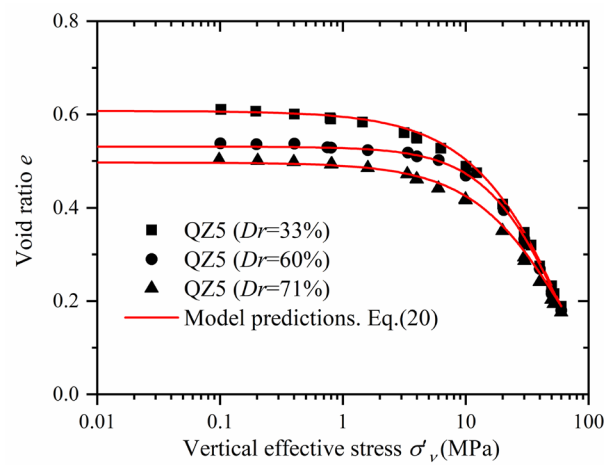
(b)



(c)

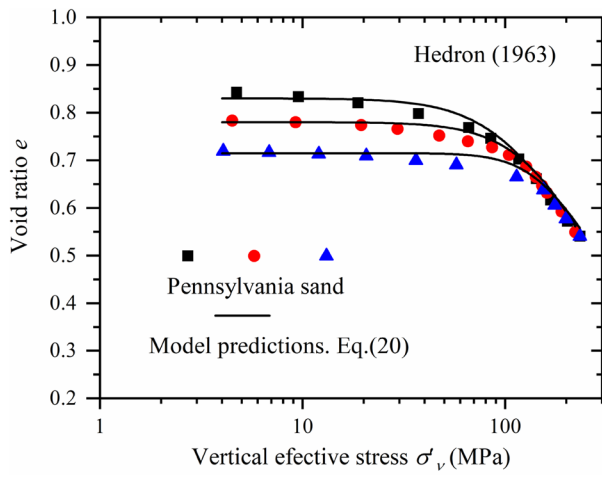


(d)

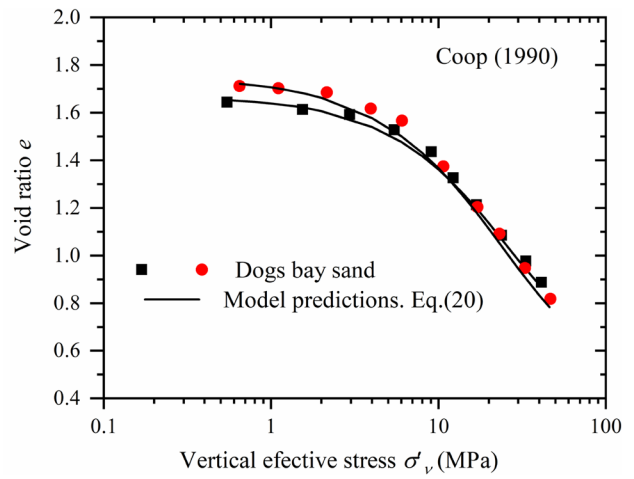


(e)

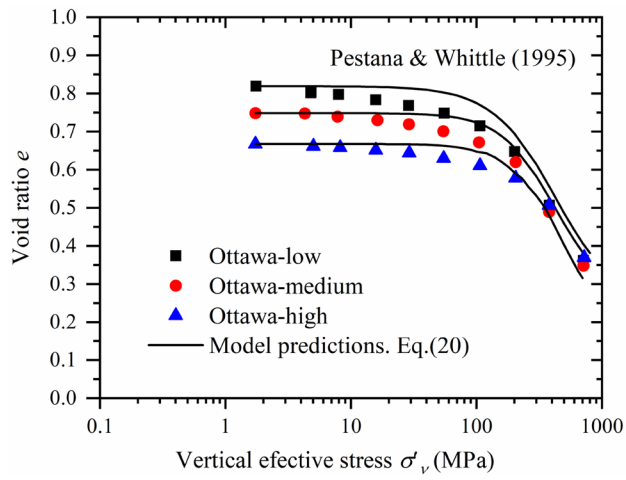
Fig. 13 Predicted one-dimensional compression lines using Eq. (20) and the experimental data for five specimens at three initial relative densities: (a) SC1; (b) SC2; (c) SC3; (d) AG4; (e) QZ5



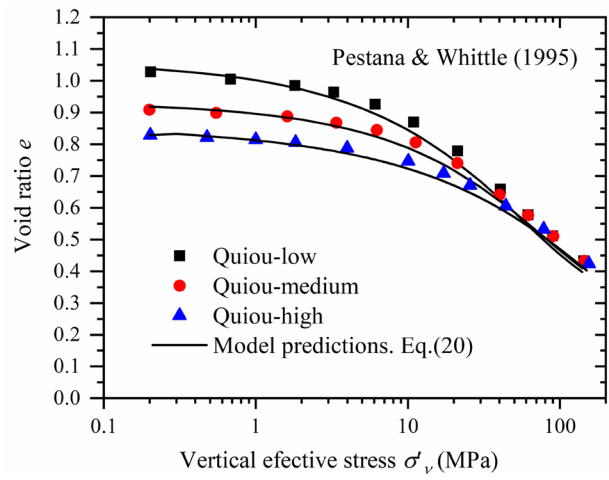
(a)



(b)

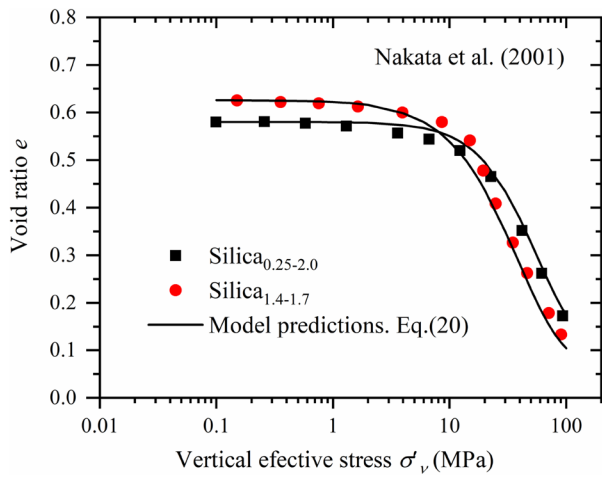


(c)

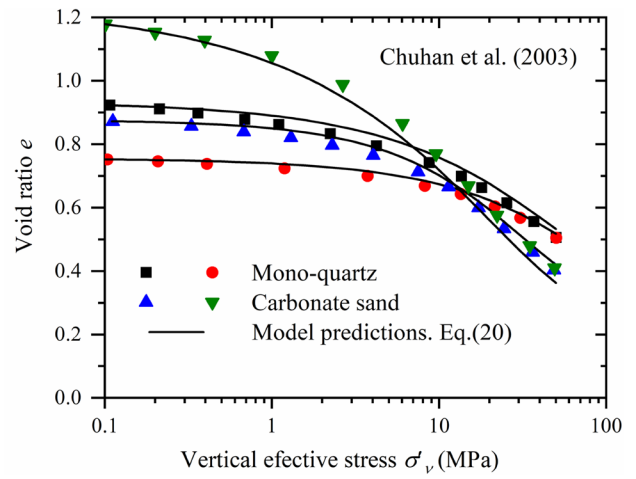


(d)

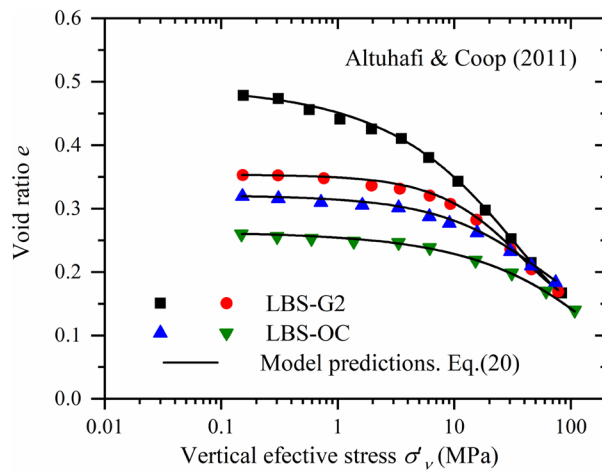
Fig. 14 Predicted compression lines using Eq. (20) and experimental data for different types of crushable sand



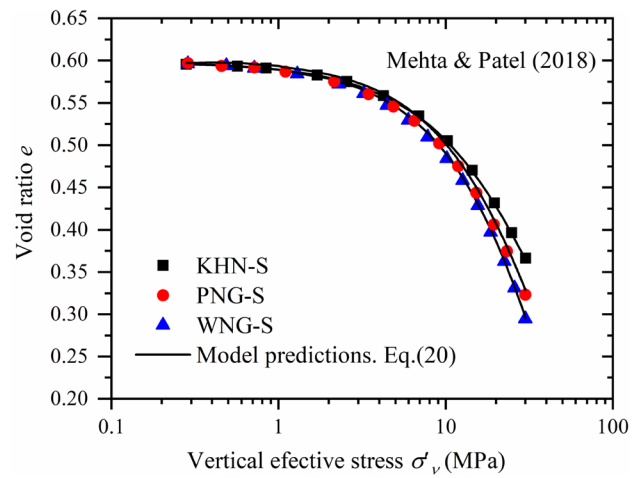
(e)



(f)



(g)



(h)

Fig. 14 (continued)

Table 6 Summary of physical properties and model parameters for selected crushable sands

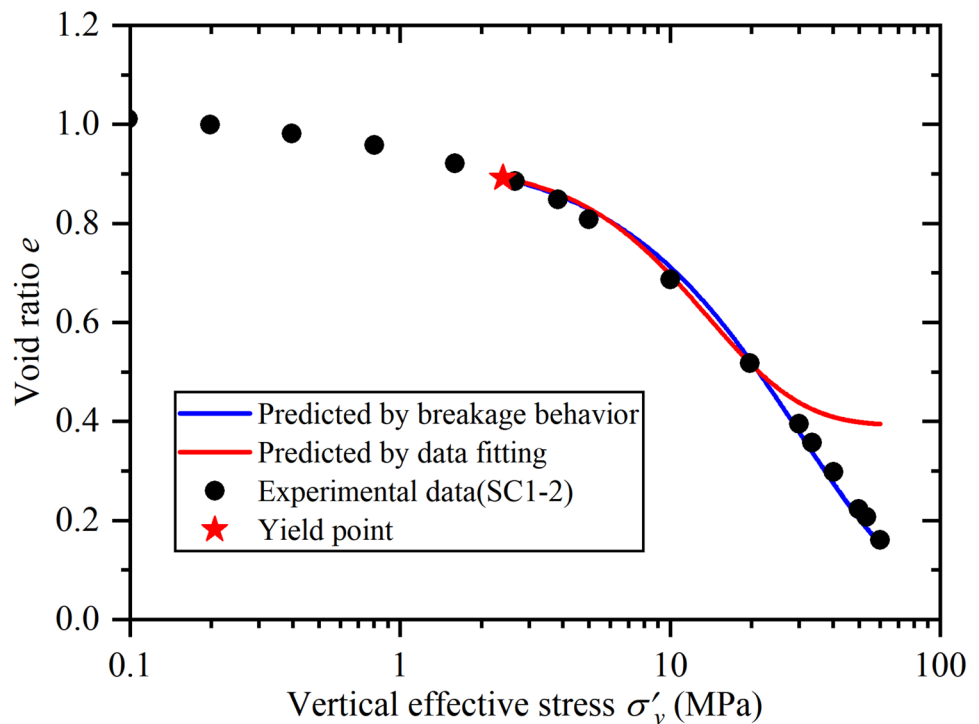
Sand name	Mineralogy	Particle shape	d_{50} (d_{60})	C_u	e_{max}	e_{min}	e_0	Model parameters			Reference
								A_t	B_t	Γ_t	
Pennsylvania sand	Q	A	1.36	1.5	0.88	0.60	0.84	44.75	0.0069	3.75	Hedron (1963)
Dogs bay sand	C	A	0.28	2.2	1.84	1.37	0.72	84.62	0.0050	3.99	Coop (1990)
Qttawa sand	Q	SR	0.14	1.5	0.83	0.63	0.72	50.75	0.0074	6.30	Pestana and Whittle (1995)
Quiou sand	Ca	A	0.70	4.5	1.20	0.78	1.65	10.95	0.0282	2.01	
Silica sand	Q	A	0.74	2.2	-	0.83	0.82	10.35	0.0287	2.10	
Mono-quartz sand	Q	R-SR	1.55 (0.71)	1.3	-	0.78	0.75	130.04	0.0025	2.92	
Carbonate sand	C	A-SA	0.19	1.7	-	0.88	1.04	116.13	0.0029	3.50	
Leighton Buzzard sand (LBS-G2) ^a	Q	R	0.84	9.8	-	0.35	0.92	22.35	0.0077	1.57	
Leighton Buzzard sand (LBS-OC) ^a	Q	R	0.24	20.0	-	0.32	0.92	27.52	0.0061	1.62	
Kanhana sand (KHIN-S) ^b	Q	R	0.77	2.9	0.77	0.48	0.83	68.35	0.0024	1.51	
Penganga sand (PNG-S) ^b	Q	A-SA	0.55	2.1	0.78	0.39	0.58	18.11	0.0187	2.86	Nakata et al. (2001)
Wannanga sand (WING-S) ^b	Q	A-SA	0.47	1.7	0.83	0.38	0.63	13.92	0.0232	2.44	Chuhan et al. (2003)
							0.74	42.16	0.0045	1.73	
							0.93	16.14	0.0098	1.63	
							0.88	10.55	0.0194	1.87	
							1.21	9.53	0.0194	1.48	
							0.48	8.51	0.0135	1.56	Altuhaifi and Coop (2011)
							0.35	6.17	0.0191	2.06	
							0.32	7.83	0.0106	1.78	
							0.26	40.16	0.0023	1.58	
							0.60	13.44	0.0169	2.07	Mehta and Patel (2018)
							0.60	27.46	0.0138	2.14	
							0.60	16.37	0.018	2.17	

Q quartz, C carbonate, Ca calcareous, A angular, R round, SA sub-angular, SR sub-round

^aThe Leighton Buzzard sand with different initial gradations

^bAbbreviations for the corresponding sands

Fig. 15 The predicted “ $e-\log\sigma'_v$ ” curves from breakage behavior and data fitting



Conclusions

This paper investigates the compression behavior and particle breakage for carbonate sands from South China Sea, Arabian Gulf, and quartz sand from Tianjin, China by conducting a series of one dimensional compression tests. The following conclusions could be inferred from the results:

1. At high stress levels, the effect of initial relative densities on compression and particle breakage decreased and eventually eliminated, which can be verified by the converging $e - \log'_v$ curves and roughly the same particle breakage extent of each specimen with three initial relative densities.
2. Compared to the quartz sand, carbonate sand is more compressible and easier to crush, which could be attributed to its angular particle shape, lower single particle strength and higher calcium carbonate content. At the same time, the more particle breakage are subjected, the greater the compressibility of the sand, because of large relative motions between sand particles resulting in large deformation.
3. The yield points for five specimens at each given relative density show that the relation between the yield stress with respect to the relative density is positively linear. In addition, the results show that the low yield stress is significative of high compressibility.
4. In order to consider the effect of particle breakage on soil compression, the relationship between W_{p2} and σ_v was

established by taking B_r as an intermediate variable, then the relationship between void ratio e and σ'_v was further obtained. This model has a good performance in predicting the compression deformation caused by crushing. It also shows that there is a close relationship between the compression deformation of sand and the plastic work.

5. For the compression deformation caused by the adjustment of particle position can also be characterized by plastic work, thus the above model further be extended to the whole compression process, that is, the same model form is adopted to describe the soil deformation in the whole compression process. By obtaining the model parameters with data fitting method, satisfying results are obtained for the available experimental data in this paper and from other literatures. But its accuracy in predicting the compressibility of soil beyond the test range needs to be further confirmed.

Funding This work was supported by the National Natural Science Foundation of China (Grant Nos. 42072294 and 51890911).

References

ASTM (1996) ASTM D243–04. Standard test methods for one-dimensional consolidation properties of soils, annual book of ASTM Standards. ASTM, Philadelphia

ASTM D854 (2014) Standard test methods for specific gravity of soil solids by water pycnometer. West Conshohocken, PA, USA

- ASTM D4253 (2016a) Standard test method for maximum index density and unit weight of soils using vibratory table. West Conshohocken, PA, USA
- ASTM D4254 (2016b) Standard test method for minimum index density and unit weight of soils and calculation of relative density. West Conshohocken, PA, USA
- ASTM D2487–17 (2017) Standard practice for classification of soils for engineering purposes (unified soil classification system). West Conshohocken, PA, USA
- ASTM C136 (2019) Standard test method for sieve analysis of fine and coarse aggregates. West Conshohocken, PA, USA
- Altuhafi FN, Coop MR (2011) Changes to particle characteristics associated with the compression of sands. *Géotechnique* 61(6):459–471. <https://doi.org/10.1680/geot.9.P.114>
- Al Hattamleh O, AlShalabi F, Al Qablan H et al (2010) Effect of grain crushing and bedding plane inclination on Aqaba sand behavior. *Bull Eng Geol Environ* 69:41–49. <https://doi.org/10.1007/s10064-009-0238-6>
- Al Hattamleh OH, Al-Deeky HH, Akhtar MN (2013) The consequence of particle crushing in engineering properties of granular materials. *Int J Geosci* 4(7):1055–1060. <https://doi.org/10.4236/ijg.2013.47099>
- Brandes HG (2011) Simple shear behavior of calcareous and quartz sands. *Geotech Geol Eng* 29(1):113–1126. <https://doi.org/10.1007/s10706-010-9357-x>
- Chuhan FA, Kjeldstad A, Bjørlykke K, Høeg K (2003) Experimental compression of loose sands: Relevance to porosity reduction during burial in sedimentary basins. *Can Geotech J* 40(5):995–1011. <https://doi.org/10.1139/T03-050>
- Clark AR, Walker BF (1977) A proposed scheme for the classification and nomenclature for use in the engineering description of middle eastern sedimentary rocks. *Géotechnique* 27(1):93–99, 366. <https://doi.org/10.1680/geot.1977.27.1.93>
- Coop M (1990) The mechanics of uncemented carbonate sands. *Géotechnique* 40(4):607–626. <https://doi.org/10.1680/geot.1990.40.4.607>
- Coop M, Lee I (1992) The behaviour of granular soils at elevated stresses. In: *Predictive soil mechanics: Proceedings of the Wroth Memorial Symposium held at St Catherine's College, Oxford*. p 186–198
- De Souza JM, Roberts JE (1958) The compressibility of sands. *Proc ASTM* 58:1269–1277
- Einav I (2007) Breakage mechanics – part I: theory. *J Mech Phys Solids* 55(6):1274–1297. <https://doi.org/10.1016/j.jmps.2006.11.003>
- Hagerty M, Hite D, Ullrich C, Hagerty D (1993) One-dimensional high-pressure compression of granular media. *J Geotech Geoenviron Eng* 119(1):1–18. [https://doi.org/10.1061/\(ASCE\)0733-9410\(1993\)119:1\(1\)](https://doi.org/10.1061/(ASCE)0733-9410(1993)119:1(1))
- Hardin BO (1985) Crushing of soil particles. *J Geotech Geoenviron Eng* 111(10):1177–1192. [https://doi.org/10.1061/\(ASCE\)0733-9410\(1985\)111:10\(1177\)](https://doi.org/10.1061/(ASCE)0733-9410(1985)111:10(1177))
- Hardin BO (1987) 1-d strain in normally consolidated cohesionless soils. *J Geotech Geoenviron Eng* 113(12):1449–1467. [https://doi.org/10.1061/\(ASCE\)0733-9410\(1987\)113:12\(1449\)](https://doi.org/10.1061/(ASCE)0733-9410(1987)113:12(1449))
- Hendron Jr A (1963) The behavior of sand in one-dimensional compression. Ph.D. thesis, University of Illinois, Urbana, Ill.
- Johnson, K.L. 1985. *Contact mechanics*. Cambridge University Press, London, UK
- Holmes A (1978) *Principles of physical geology*. Nelson, London: Sunbury-on-Thames, p 730
- Jaeger JC (1967) Failure of rocks under tensile conditions. *Int J of Rock and Mining Science* 4:219–227
- Kikumoto M, Wood DM, Russell A (2010) Particle crushing and deformation behaviour. *Soils Found* 50(5):767–767. <https://doi.org/10.3208/sandf.50.547>
- Ladd R (1978) Preparing test specimens using undercompaction. *Geotech Test J* 1(1):16–23. <https://doi.org/10.1520/GTJ10364J>
- Lade PV, Yamamuro JA, Bopp PA (1996) Significance of particle crushing in granular materials. *J Geotech Geoenviron Eng* 122(4):309–316. [https://doi.org/10.1061/\(ASCE\)0733-9410\(1996\)122:4\(309\)](https://doi.org/10.1061/(ASCE)0733-9410(1996)122:4(309))
- Lin L, Li S, Sun L, Liu X, Chen W (2020) Evolution of particle size distribution for carbonate sand under impact load. *Powder Technol* 376:549–564. <https://doi.org/10.1016/j.powtec.2020.08.046>
- McDowell G, Bolton M (1998) On the micromechanics of crushable aggregates. *Géotechnique* 48(5):667–679. <https://doi.org/10.1680/geot.1998.48.5.667>
- McDowell GR, Amon A (2000) The application of Weibull statistics to the fracture of soil particles. *Soils Found* 40(5):133–141
- McDowell GR (2002) On the yielding and plastic compression of sand. *Soils Found* 42(1):139–145. <https://doi.org/10.3208/sandf.42.139>
- Mehta AA, Patel A (2018) An investigation on the particle breakage of indian river sands. *Eng Geol* 233:23–37. <https://doi.org/10.1016/j.enggeo.2017.12.001>
- Meidani M, Chang CS, Deng Y (2017) On active and inactive voids and a compression model for granular soils. *Eng Geol* 222:156–167. <https://doi.org/10.1016/j.enggeo.2017.03.006>
- Mesri G, Vardhanabhuti B (2009) Compression of granular materials. *Can Geotech J* 46(4):369–392. <https://doi.org/10.1139/T08-123>
- Miura N, Sukeo O (1979) Particle-crushing of a decomposed granite soil under shear stresses. *Soils Found* 19(3):1–14. https://doi.org/10.3208/sandf1972.19.3_1
- Mohs F (1825) *Treatise on mineralogy*. Mercury Press, Edinburgh
- Mun W, Mc Cartney JS (2017) Roles of particle breakage and drainage in the isotropic compression of sand to high pressures. *J Geotech Geoenviron Eng* 143(10):04017071. [https://doi.org/10.1061/\(ASCE\)GT.1943-5606.0001770](https://doi.org/10.1061/(ASCE)GT.1943-5606.0001770)
- Nakata Y, Hyde AFL, Hyodo M, Murata H (1999) A probabilistic approach to sand particle crushing in the triaxial test. *Géotechnique* 49(5):567–583
- Nakata Y, Kato Y, Hyodo M, Hyde AF, Murata H (2001) One-dimensional compression behaviour of uniformly graded sand related to single particle crushing strength. *Soils Found* 41(2):39–51. https://doi.org/10.3208/sandf.41.2_39
- Pestana JM, Whittle A (1995) Compression Model for Cohesionless Soils *Géotechnique* 45(4):611–631. <https://doi.org/10.1680/geot.1995.45.4.611>
- Roberts JE (1965) Sand compression as a factor in oil field subsidence. Ph.D. thesis, Massachusetts Institute of Technology, Cambridge, Mass
- Semple RM (1988) The mechanical properties of carbonate soils. *International conference on calcareous sediments*. Rotterdam, Perth, WA: Balkema, p 807–836
- Wang C, Ding X, Yin ZY et al (2021) Mechanical characteristics and particle breakage of coral sand under one-dimensional repeated loading. *Acta Geotech*. <https://doi.org/10.1007/s11440-021-01381-9>
- Wils L, Van Impe P, Haegeman W (2015) One-dimensional compression of a crushable sand in dry and wet conditions. *Proc., 3rd International Symposium on Geomechanics from Micro to Macro*, Taylor and Francis Group-London, p 1403–1408
- Wu JP, Chu Y, Lou ZG (1997) Influence of particle breakage on deformation and strength properties of calcareous sands [in Chinese]. *Chinese J Geotech Eng* 19(5):49–55
- Xiao Y, Liu H (2017) Elastoplastic constitutive model for rock-fill materials considering particle breakage. *Int J Geomech* 17(1):04016041. [https://doi.org/10.1061/\(ASCE\)GM.1943-5622.0000681](https://doi.org/10.1061/(ASCE)GM.1943-5622.0000681)
- Xiao Y, Liu H, Chen Q, Ma Q, Xiang Y, Zheng Y (2017) Particle breakage and deformation of carbonate sands with wide range

- of densities during compression loading process. *Acta Geotech* 12(5):1177–1184. <https://doi.org/10.1007/s11440-017-0580-y>
- Xiao Y, Meng M, Daouadji A, Chen Q, Wu Z, Jiang X (2020) Effects of particle size on crushing and deformation behaviors of rockfill materials. *Geosci Front* 11(2):375–388. <https://doi.org/10.1016/j.gsf.2018.10.010>
- Yan W, Shi Y (2014) Evolution of grain grading and characteristics in repeatedly reconstituted assemblages subject to one-dimensional compression. *Géotech Lett* 4(3):223–229. <https://doi.org/10.1680/geolett.14.00039>
- Yu FW (2017) Characteristics of particle breakage of sand in triaxial shear. *Powder Technol* 320:656–667. <https://doi.org/10.1016/j.powtec.2017.08.001>
- Zhang J, Wong TF, Davies DM (1990) Micromechanics of pressure-induced grain crushing in porous rocks. *J Geophys Res* 95(B1):341–352. <https://doi.org/10.1029/jb095ib01p00341>
- Zhou XZ, Chen YM, Liu HL, Zhang XL (2019) Experimental study on the cyclic behavior of loose calcareous sand under linear stress paths. *Mar Georesources Geotechnol* 1–14. <https://doi.org/10.1080/1064119X.2019.1567631>